Review Paper

Analytical models for high-temperature corrosion of silica refractories in glass-melting furnaces

Robert H. Nilson, Stewart K. Griffiths, Nancy Yang, Peter M. Walsh and Mark D. Allendorf

Sandia National Laboratories, Livermore, CA (USA)

Benjamin Bugeat and Ovidiu Marin

Chicago Research Center, American Air Liquide, Countryside, IL (USA)

Karl E. Spear

Department of Materials Science and Engineering, Pennsylvania State University, University Park, PA (USA)

George Pecoraro

PPG Industries Inc., Glass Technology Center, Pittsburgh, PA (USA)

Corrosion of refractory silica brick used to line the crown of many glass-melting furnaces is a serious problem in furnaces using oxygen-fuel rather than air-fuel mixtures. To better understand and to quantify this process analytical models are utilized to evaluate the importance of four potential rate-limiting processes: a) gas-phase transport of NaOH to the crown surface; b) diffusion of sodium-containing reactants through a liquid product layer that forms on the brick face; c) gas-phase diffusion of NaOH into refractory pores; and d) chemical-kinetic limitations at the silica grain surface. Predictions are compared with reported corrosion rates and product compositions previously determined by post-mortem analysis of refractory samples. It is concluded that corrosion occurs largely by reaction and removal of material from the exposed brick face, rather than by transport of reactants into the porous bricks. The observed presence of corrosion products deep within the brick pores is shown to be consistent with capillary suction of high-viscosity liquid products from the hot face into the interior. The results further suggest that mechanisms (b) and (c) do not substantially limit the rate of corrosion, but that mechanisms (a) and (d) may both be important. Comparison of measurements with equilibrium predictions of corrosion-product composition indicate that the corrosion reactions are likely to be close to equilibrium at the conditions and lifetimes typical of full-scale furnaces, but that significant departures from equilibrium may occur in short-duration tests. Although computed corrosion rates based on mass transport through a gas boundary layer are somewhat greater than those observed, the results are very sensitive to the gas-phase concentration of NaOH and to the refractory temperature, both of which contain significant uncertainties.

1. Introduction

Corrosion of silica-containing refractories used to line the crown of glass-melting furnaces is a problem that has been known for some time. Chemically, corrosion of silica occurs when water reacts with components in the glass melt, typically Na_2O or K_2O, to produce gas-phase NaOH(g) or KOH, which is then transported to the refractory surface. The hydroxide can react with silica to form a low-melting alkali-silicate product:

$$2MOH(gas) \leftrightarrow M_2O(\text{dissolved in liquid } SiO_2) + H_2O(gas)$$

where M = Na or K.

Received 25 July 2002, revised manuscript 6 January 2003.

This product can be absorbed into the pores of the refractory and/or drip and run down the sides of the furnace. The exact process that controls the corrosion rate is unknown. Potential candidates include (figure 1): gas-phase mass transport of MOH; transport of sodium through the liquid layer to the surface of the refractory; chemical kinetics at the silica surface; and diffusion of NaOH(g) through pores in the refractory, which we will term "in-depth" corrosion.

Early investigations going back to at least the early 1960s describe the formation of glassy corrosion products composed of sodium silicates. Work by Reich [1] and Morsanyi [2 and 3] characterized this process in air-fired furnaces and showed that the glassy phase migrates toward the cold end of porous refractory blocks; the importance of temperature gradients in the refractory was noted as well. Two general phenomena were observed in large-scale fur-

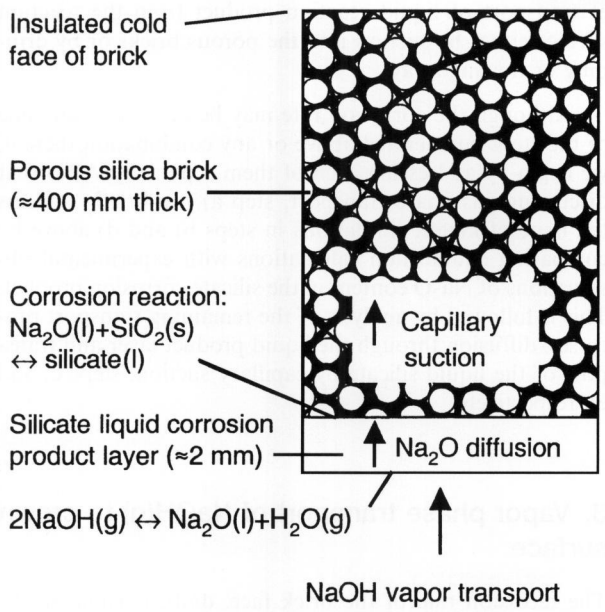

Figure 1. Schematic of corrosion process. A thin (≈2 mm) layer of liquid reaction product coats brick surface. NaOH(g) vapor is transported to the lower surface of the liquid, releases H_2O to form $Na_2O(l)$ that diffuses through liquid layer to surface of solid SiO_2 grains. Reaction of Na_2O with SiO_2 forms additional silicate liquid that is drawn into the porous brick by capillary suction.

naces: front-face corrosion, in which the surface of the refractory was eroded over time, and so-called "ratholing", in which narrow channels at joints or gaps were invaded by combustion gases, creating wider channels and interior chambers in colder regions of the brick. In air-fired furnaces, the latter was a severe problem until the 1960s, when furnace crowns were insulated, virtually eliminating the problem [4]. Front-face corrosion is sufficiently slow in air-fired furnaces that crown lifetimes of up to ten years can be achieved, which is an acceptable rate of degradation.

The advent of oxy-fuel melting technologies in the late 1980s and early 1990s caused silica corrosion to again become a major concern to the glass industry and led to efforts to understand and predict corrosion as a function of furnace conditions. The replacement of air with oxygen, although attractive from a number of standpoints [5], causes crown corrosion rates to increase by as much as a factor of two, reducing furnace lifetimes to five years or less in some cases. Numerous qualitative investigations using sophisticated analytical methods, including works by Paskocimas et al. [6], Kotacska and Cooper [7], Boillet et al. [8 and 9], Faber and Verheijen [10], Godard et al. [11], and Duvierre et al. [12], show that many of the features of silica corrosion in air-fired furnaces are also seen under oxy-fuel conditions. For the most part, these investigators reached the same conclusions concerning strategies for reducing corrosion; however, none attempted to quantitatively predict corrosion rates. The accelerated degradation of the refractory front face is the principal symptom, rather than ratholing, as was the case in air-fired furnaces. Qualitatively, the cause of the faster corrosion seems easy to understand: the increased concentration of oxygen in the furnace produces much higher partial pressures of water vapor (up to) 0.67 for stoichiometric methane/oxygen – 0.65 has been observed – versus 0.18 for an air-fired furnace [13], leading to higher gas-phase alkali concentrations and thus an accelerated rate of the above reaction.

In spite of these extensive efforts, there have been very few attempts to develop quantitative models that can predict corrosion rates as a function of furnace conditions. Wu and Kobayashi modeled crown corrosion in the mass transport limit (i.e., assuming that corrosion is limited by the rate of vapor-phase transport of NaOH(g) to the refractory surface), which represents the upper limit for the process [14]. Their model uses computational fluid dynamics (CFD) to simulate the three-dimensional combustion processes and to assess the effects of burner elevation on alkali volatilization. Only relative crown corrosion rates were reported, so it cannot be determined whether the mass transport limit is in fact close to observed corrosion rates. Most details of the model are not provided, making it difficult to make direct comparisons with other models. Misra et al. developed a similar model, again using CFD calculations to predict velocity and temperature fields in the combustion space over the glass [15]. Simplified chemical reactions were also employed, using empirically estimated rate constants. The results are evidently in quantitative agreement with observation, although no direct comparisons are shown. The authors also point out the need to include thermodynamics of the equilibrium between the combustion gases and liquid-phase corrosion products. While the success of this effort is tantalizing, the lack of specifics again inhibits further development; for example, none of the rate constants used to model the corrosion reactions are reported. Allendorf and Spear recently established thermodynamic data for the variable-composition sodium-silicate products and predicted equilibrium NaOH(g) concentrations for air- and oxy-fired conditions as a function of temperaturef [16]. These results were used to identify concentration and temperature regimes under which silica corrosion is thermodynamically favorable. Walsh et al. made further use of these data and earlier approximations thereof [17] to calculate corrosion rates limited by gas-phase transport of NaOH in a manner very similar to that used in the present paper [18 and 19]. However, none of these investigations allow firm conclusions to be drawn about which of the four processes described above is the rate-controlling step.

Quantitative measurements of furnace conditions critical to model validation, such as refractory temperature, gas-phase alkali concentrations, and actual corrosion rates, are scarce. One of the most thorough investigations is by Faber and Beerkens [17], who measured NaOH (g) concentrations in several glass furnaces. Concentrations of 50 to 60 ppm in an air-fired furnace were observed (13 wt% soda in the glass), 140 to 200 ppm in an oxy-fired furnace with a comparable soda-lime-silica glass, and 220 to 260 ppm in an oxy-fired furnace melting soda-lime-silica glass with 16 wt% soda. Anecdotal NaOH(g) concentrations for oxy-fired furnaces range from 100 to 250 ppm: these results are consistent with measurements by Walsh et al. based on atomic-sodium absorption spectroscopy [20]. Faber and Beerkens also exposed refractory test samples to controlled furnace atmospheres and measured Na_2O concentration profiles as a function of temperature and distance from the hot face. They correlated these results with thermodynamic modeling that apparently accounted for the variable-composition liquid corrosion products, although the source of the

thermodynamic data for these liquid products is not given, and no conclusions are drawn regarding the rate-limiting process. Finally, corrosion rates are reported by Tong et al. (who also report gas-phase alkali concentrations) [13]. These limited studies emphasize the need for additional measurements of corrosion rates under controlled, or at least well characterized, conditions.

The objective of this work is to use analytical models to predict rates of silica corrosion by NaOH(g) that result from each of the four processes listed above and use these results to determine which is most likely to be the rate-limiting mechanism. We consider only front-face corrosion and do not deal specifically with ratholing, a mechanism suggested in a previous paper [16]. However, some of the phenomena occurring during the formation of rat holes are examined here and could potentially be of value in modeling this process and other types of in-depth corrosion. Model results are compared with three types of data: a) chemical analysis of silica refractories exposed to corrosive atmospheres in a laboratory furnace; b) post-mortem analysis (corrosion rates and chemical analysis) of samples taken from a container-glass furnace; and c) data reported in the literature (see above). Although this paper focuses on silica, the analysis of the various corrosion processes that could occur is applicable to any refractory and can be made quantitative if thermodynamic data are available describing the equilibrium between a gas-phase corrosive species and the refractory of interest. It is also likely that the qualitative conclusions of this analysis can be directly extended to corrosion of silica by KOH(g), whose equilibrium with silica is similar to that of NaOH(g) [16]. However, little is known about KOH(g) concentrations or about the presence of potassium-containing corrosion products within silica bricks, so we will not discuss this further.

2. Phenomenology of corrosion

Corrosion of silica will occur at the exposed crown surface whenever the gas-phase concentration of NaOH(g) exceeds the value associated with local equilibrium between the gas, the solid SiO_2, and the sodium-containing liquid reaction product (reaction in section 1) [16]. The surface corrosion process thus involves transport of NaOH(g) from the furnace atmosphere to refractory surfaces where these reactants combine to form a sodium silicate product. Since the silica reaction product is a high-viscosity liquid at typical furnace conditions, some of it may be drawn into the pores of the brick by capillary suction or drip from the surface, but at least part of it remains as a thin layer that coats the external surface of the brick. Thus, as illustrated schematically in figure 1, the quasi-steady surface corrosion process may be viewed as a series of distinct steps:

a) transport of NaOH(g) vapor from the furnace gas to the external surface of the liquid product layer that coats the crown surface,

b) formation of Na_2O at the external surface of the liquid product layer,

c) diffusion of Na_2O through the liquid product layer to the SiO_2 surface,

d) dissolution of silica to form a sodium-rich silicate at the interface between the liquid product and the unreacted silica grains,

e) transport of liquid reaction product from the reaction surface either by suction into the porous bricks or by dripping or flowing away.

Although the corrosion rate may be limited by any one of the steps enumerated above or any combination thereof, we begin by addressing each of them separately. After first discussing gas-phase transport, step a), we briefly address the issue of kinetic limitations in steps b) and d) above by comparing equilibrium calculations with experimental observations of Na_2O content in the silicate corrosion product. This is followed by analysis of the remaining transport processes, diffusion through the liquid product layer and transport of the liquid silicate by capillary suction, steps c) and e), respectively.

3. Vapor phase transport of NaOH(g) to crown surface

The recession rate of the brick face, dl/dt, is equal to the areal reaction rate of SiO_2, $\dot{n}_{SiO_2}$ (mol/(s·m^2)), divided by the molar density of SiO_2 in the unreacted brick, ϱ_{SiO_2}. In addition, the number of moles of SiO_2 eroded by one mole of NaOH(g) is $(1 - x)\cdot 2/x$, where x is the mole fraction of Na_2O in the melt and the factor of two accounts for the fact that two moles of NaOH(g) are reacted to form each mole of Na_2O. Thus, the recession rate, dl/dt, may be written as follows in terms of the reaction rate of the NaOH(g), $\dot{n}_{NaOH}$.

$$\frac{dl}{dt} = \frac{\dot{n}_{SiO_2}}{\varrho_{SiO_2}} = \left(\frac{1-x}{2x}\right)\frac{\dot{n}_{NaOH}}{\varrho_{SiO_2}} . \tag{1}$$

In a quasi-steady process, the reaction rate of the sodium must be in balance with the transport of NaOH(g) from the furnace gas to the refractory surface. The latter of these may be expressed as the rate of diffusion through a gas boundary layer having a mean thickness, $\delta_g = L/Sh$, where L is the length of the flow path over the surface and Sh is the Sherwood number.

$$(\dot{n}_{NaOH})_{reaction} \approx (\dot{n}_{NaOH})_{transport} \tag{2}$$

$$= \varrho_g \Delta X \frac{D}{\delta_g} = \varrho_g \Delta X \, Sh \frac{D}{L} .$$

Here ϱ_g is the molar density of the furnace gas, D is the gas-phase diffusivity of the NaOH(g), L is the length scale of the furnace, and ΔX is the difference in NaOH(g) concentration (mole fraction) across the gas-phase boundary layer adjacent to the crown face.

$$\Delta X = X_{amb} - X_{g,l} \approx X_{amb} - X_{eq} . \tag{3}$$

In general, ΔX is the difference between the ambient mole fraction outside the boundary layer, X_{amb}, and that immediately adjacent to the gas-liquid interface, $X_{g,l}$, on the crown surface. Both of these quantities may vary considerably over the crown. If there are no rate limitations imposed by reaction kinetics or by diffusion through the liquid product layer, the NaOH(g) concentration in the gas immediately adjacent to the melt should be equal to the equilibrium con-

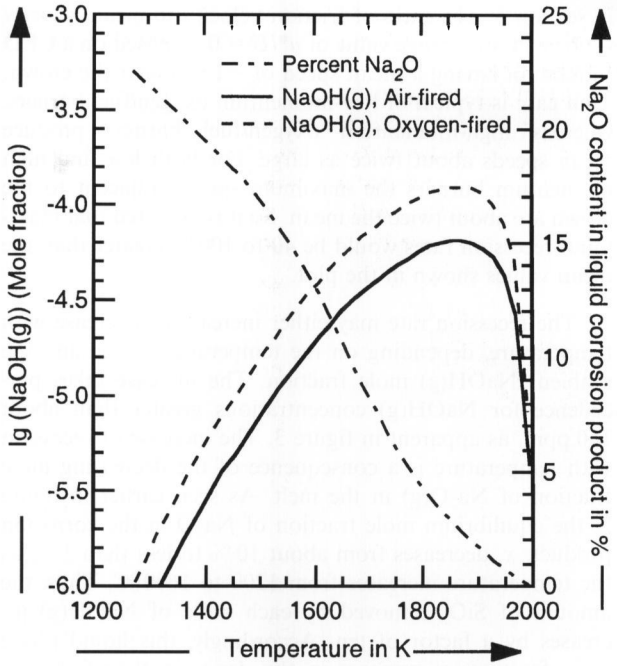

Figure 2. Mole fraction of NaOH(g) in equilibrium with silica as a function of temperature under oxy-fuel and air-fuel conditions. In both cases, O_2/CH_4 mole ratio = 2.05. Also shown is the equilibrium concentration of Na_2O dissolved in the liquid-phase corrosion product as a function of temperature. Data are taken from Allendorf and Spear [16].

centrations, X_{eq}, displayed in figure 2. Corrosion occurs whenever $X_{amb} > X_{eq}$, and the resulting corrosion rate is proportional to $\Delta X = X_{amb} - X_{eq}$.

$$\frac{dl}{dt} = \frac{\varrho_{gas}}{\varrho_{SiO_2}} \Delta X \, Sh \frac{D}{L} \left(\frac{1-x}{2x} \right). \tag{4}$$

The Sherwood number, Sh, may be interpreted either as a ratio of length scales, L/δ_g, or as the ratio of the actual transport through the boundary layer to that which would occur by diffusion through the length scale, L. Sh is much greater than unity in most applications. Three different models are used to estimate the magnitude of the Sherwood number: a) laminar flow over a flat surface, b) turbulent flow over a flat surface, and c) analysis of numerical CFD results (see section 8). The well known laminar relation and the Coburn formula for turbulent flow of a gas (Schmidt number (Sc) near unity) depend on the Reynolds number, Re, as indicated below [21].

$$Sh_{lam} = 0.66 \, Re^{0.5} \tag{5}$$

$$Sh_{turb} = 0.037 \, Re^{0.8} \tag{6}$$

$$Re = \frac{\bar{\varrho}_g \, UL}{\mu_g}. \tag{7}$$

Here U is the gas speed adjacent to the surface, μ is the gas viscosity, and $\bar{\varrho}_g = \bar{M}\varrho_g$ is the mass density based on the mean molecular weight, $\bar{M}$. The third estimate of Sh is derived from CFD contour plots of the gas speed ($\approx$ 1 to 2 m/s for oxy-fuel) adjacent to the crown as well as corresponding contours of the friction velocity, u^*. The latter quantity is a direct indication of the shear stress, τ, on the adjacent crown surface and is, thus, related to the friction factor, f.

$$u^* = \sqrt{\frac{\tau}{\bar{\varrho}_g}} \tag{8}$$

$$f = \frac{2\tau}{\bar{\varrho}_g \, U^2}. \tag{9}$$

Further, by the Reynolds analogy between mass and momentum transfer [21], the friction factor is related to the mass flux, j_D, and mass transfer coefficient, h_D, which are simply related to the Sherwood number and the Schmidt number (Sc is roughly unity for gases) to obtain the needed relationship between the Sherwood number and the U and u^* values from the CFD model.

$$j_D = \frac{f}{2} = \frac{h_D}{U} Sc^{2/3} \tag{10}$$

$$Sh = h_D \frac{L}{D} \tag{11}$$

$$Sh_{fric} = \left(\frac{u^*}{U} \right)^2 \frac{UL}{D}. \tag{12}$$

The gas density, viscosity, and diffusivity appearing in the above formulas are evaluated using the ideal gas law, the Sutherland formula [22], and a well known approximation derived from the molecular theory of gasses [23].

$$\varrho_g = \frac{P}{R\,T} \tag{13}$$

$$\frac{\mu}{\mu_0} = \left(\frac{T}{T_0} \right)^{1/2} \tag{14}$$

$$D = \frac{2.6 \cdot 10^{-22}}{P \, \sigma_{12}^2} \sqrt{\frac{T^3}{m_{12}}}. \tag{15}$$

Here, P and T are the gas pressure and temperature, R is the gas constant, and T_0 is the temperature corresponding to the reference value of the viscosity, μ_0. The mean molecular weight and diameter appearing in equation (15) are respectively computed from those of the diffusing species and the bulk gas mixture as $m_{12} = 2m_1m_2/(m_1 + m_2)$ and $\sigma_{12} = (\sigma_1' + \sigma_2)/2$. Based on the preceding analytical relationships and values of X_{eq} and x displayed earlier in figure 2, the recession rate can now be evaluated for typical furnace conditions.

Figure 3 shows computed recession rates versus crown temperature for various NaOH(g) concentrations in an oxy-fuel furnace having an H_2O concentration of 65 %. Recession rates indicated by solid lines utilize the turbulent flow estimate of the Sherwood number. Comparative estimates based on laminar flow (dotted) and the CFD friction velocities (chain-dotted) are shown for NaOH(g) concentrations of 50 and 150 ppm. In these and all other cases the analytical results for laminar and turbulent flow differ by

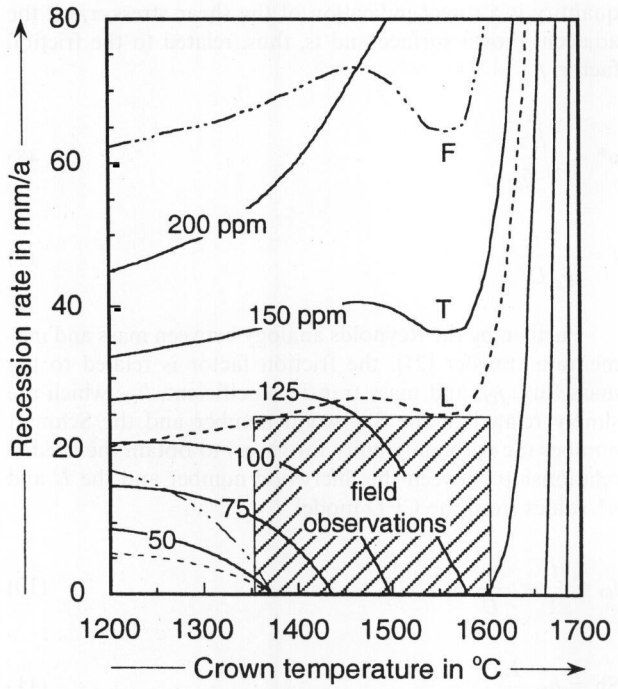

Figure 3. Computed recession rates for oxy-fuel combustion. Gas velocity and flow path length are U = 1.5 m/s and L = 5 m. Mole fraction of NaOH(g) in furnace gas is taken at 50, 75, 100, 125, 150, and 200 ppm. Solid lines indicate results for turbulent flow (T) model. Dotted and chain-dotted lines shown only for 150 and 50 ppm indicate results for laminar (L) and friction-based (F) models of mass transfer rate. Shaded box represents approximate range of field observations.

less than 30 %, mainly because the Reynolds number of about 30 000 is transitional, on the borderline between laminar and turbulent flow. The estimates based on the CFD friction velocities are about twice as great, perhaps because they better reflect the furnace-scale turbulence induced by the burner jets.

The most important conclusion to be drawn from figure 3 is that computed recession rates for large but credible NaOH(g) concentrations of 150 to 200 ppm are generally greater than those observed in oxygen/fuel furnaces. For example, at a crown temperature of 1550 °C, concentrations of 150 to 200 ppm produce computed recession rates of 40 to 100 mm/a (60 to 150 mm/a based on CFD friction) as compared with anectodal observations of about 25 mm/a (although a value much higher than this – 100 mm/a – has been reported [10]) This rate (25 mm/a) corresponds to the top of the shaded box at the bottom of the plot; the sides of the box roughly indicate the typical range of crown temperatures, 1350 to 1650 °C. The computed recession rates would be consistent with these observations if the NaOH(g) concentration is no greater than 125 ppm. One report we are aware of, however, indicates that NaOH(g) concentrations as high as 350 to 400 ppm can be produced by unfavorable burner orientation in an oxy-fuel furnace [24]. Such large concentrations yield calculated recession rates greatly exceeding even the (presumably atypical) 100 mm/a observed by Faber and Verheijen in a low-temperature area above the batching area [10].

The gas velocity and length scale used to construct figure 3 are U = 1.5 m/s and L = 5 based on the CFD results in section 8. The ratio of friction velocity to mean velocity is taken at an average value of $u^*/U \approx 0.12$ based on a CFD simulation having a mean speed of ≈1 m/s near the crown. That case is typical of low-momentum oxygen/fuel burners, whereas high-momentum oxygen/fuel burners produce mean speeds about twice as large. For both low and high momentum burners the maximum speeds adjacent to the crown are about twice the mean. So it is expected that maximum recession rates would be 40 to 100 % greater than the mean values shown in the plot.

The recession rate may either increase or decrease with temperature, depending on the temperature range and the ambient NaOH(g) mole fraction. The increase takes precedence for NaOH(g) concentrations greater than about 150 ppm, as apparent in figure 3. The increase of recession with temperature is a consequence of the decreasing mole fraction of Na_2O(g) in the melt. As seen earlier in figure 2, the equilibrium mole fraction of Na_2O in the corrosion product, x, decreases from about 10 % to less than 1 %, as the temperature increases from 1200 to 1600 °C. Thus, the amount of SiO_2 removed by each mole of NaOH(g) increases by a factor of ten. Accordingly, this liquid phase mole fraction, x, appears in the denominator of the expression for the recession rate in equation (4).

For smaller values of the ambient NaOH(g) concentration, X < 125 ppm in figure 3, the recession rate decreases with temperature up to a temperature of about 1600 °C. This results from the increase of the equilibrium gas-phase concentration, X_{eq}, with temperature, as illustrated earlier in figure 2. The increase in X_{eq} helps to reduce the concentration difference $\Delta X = X - X_{eq}$, that drives the diffusive flux of NaOH(g) through the boundary layer to the crown surface. Note that ΔX appears in the numerator of equation (4). However, this downward trend reverses above 1600 °C because the equilibrium vapor phase concentration then decreases with temperature. At high temperatures this increase in ΔX reinforces the decreasing liquid-phase mole fraction to produce the extremely large recession rates seen on the right side of figure 3. These same trends are seen in the results of figure 4 which apply to air-fuel combustion.

Figure 4 compares computed and observed surface recession rates for air-fuel combustion. It is very similar to the earlier figure 3 for oxygen-fuel combustion and, as before, computed recession rates are somewhat greater than those generally observed. For air-fuel combustion, the computed recession rate for 75 ppm NaOH(g) is around 20 mm/a. Well-insulated crowns of air-fuel furnaces usually recede much more slowly than this. For comparison, Wereszczak et. al. report recession of only 6 mm in 10 years of exposure at 1600 °C in a soda-lime-silica float-glass furnace and 13 mm recession in 6.5 years at 1600 °C in a TV-panel glass furnace [25]. Thus, we take 2.5 mm/a (≈25 mm/10 years) as a typical air-fuel recession rate corresponding to the top of the gray box in figure 4. Faber and Verheijen report considerably greater recession rates, ranging from 5 to 10 mm/a at 1530 to 1580 °C, but the larger value is for a brick located over the batch area where NaOH(g) concentrations are expected to be greatest, probably greater than 75 ppm [10]. For comparison, the computed recession rate for 100 ppm NaOH(g) is around 40 mm/a, about four times greater than the observation. Moreover, the calculations in figure 4 utilize a mean speed of only 1.5 m/s, which is about a factor of two smaller than those measured by Webb near the crown

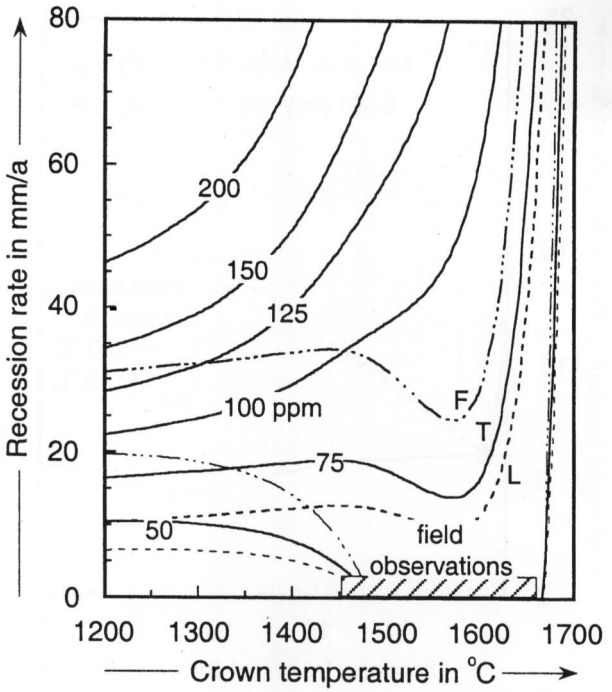

Figure 4. Computed recession rates for air-fuel combustion. Gas velocity and flow path length are U = 1.5 m/s and L = 5 m, the same as in the preceding plot for oxy/fuel combustion. The difference in recession rates between air and oxygen supported combustion is caused mainly by the difference in equilibrium thermodynamics resulting from different H_2O concentrations in the furnace gas. Solid lines indicate results for turbulent flow (T) model. Dotted and chain-dotted lines shown only for 50 and 75 ppm indicate results for laminar (L) and friction-based (F) models of mass transfer rate.

of an air-fuel furnace [26]. Use of a larger velocity would increase the disparity between observed and computed recession rates.

Although computed recession rates based on gas-phase transport appear to exceed observations, the results are very sensitive to NaOH concentrations and crown surface temperature which are not accurately known. Moreover, it is very encouraging to see that computed recession rates do decrease with crown temperature for sufficiently small values of the ambient NaOH(g) concentration. This result is consistent with industry experience showing that elevation of the crown temperature by addition of thermal insulation to the backside of the refractory greatly reduces corrosion. Thus, it is likely that the operative physics are correctly modeled, but that some of the inputs to the analysis may be inaccurate. For example, NaOH(g) concentrations in field operations may be a factor of two less than the conventional estimates of ≈200 ppm for oxy-fuel and 40 to 80 ppm for air-fuel. Alternatively, our current estimates of NaOH(g) equilibrium values, $X_{eq}(T)$, may be low by 20 to 30 %. Another possibility is that our estimates of the Na_2O concentration in the melt, $x_{eq}(T)$, are too low. Any of these explanations or some combination thereof could bring the predictions into better agreement with the data. Another possibility is that some other transport or kinetic limitation is controlling the corrosion rate. For that reason we explore some alternative rate-limiting mechanisms.

4. Kinetics of reaction at liquid/grain interface

In general, concentration differences for sodium-containing species are needed to drive the reactions occurring on both sides of the liquid product layer as well as the sodium transport through both the gas and the liquid. However, one of these processes is often much slower than the others and so consumes most of the available difference between the sodium concentration in the ambient gas and that associated with full equilibrium between the solid, liquid, and gas at a given temperature. In the analysis of the preceding section it is assumed that the reaction kinetics are fast and the diffusivity of Na_2O in the liquid is large. Under these conditions the liquid product layer will be nearly in equilibrium with the solid SiO_2 ($x \approx x_{eq}$) and with the gas immediately adjacent to the liquid. All of the NaOH concentration difference between the ambient gas and the gas immediately adjacent to the liquid is then available to drive the transport through the boundary layer.

To assess the influence of reaction kinetics let us accept that the Na_2O diffusivity is large (as will be demonstrated in the next section) and suppose that the reaction kinetics is slow. If this is the case, the silicate liquid layer would approach equilibrium with the ambient gas phase, and the Na_2O concentration in the liquid adjacent to the solid SiO_2 grains would exceed the value corresponding to equilibrium with the solid ($x > x_{eq}$); this concentration difference drives the silica dissolution reaction. The resulting increase in the sodium content of the melt, x, and the consequent reduction in the gas-phase concentration gradient, $\Delta X/\delta_g$, would then reduce the recession rate computed from equation (4), bringing the predictions into better agreement with field observations. This hypothesis can be tested by comparing measured values of the Na_2O mole fraction in the silicate corrosion product with those predicted by modeling the equilibrium thermodynamics.

To make this comparison, the equilibrium Na_2O mole fraction in the sodium-containing liquid corrosion product was calculated as a function of the vapor-phase NaOH(g) mole fraction for two cases, using the ChemSage program (27 and 28) and the SiO_2/Na_2O thermochemistry reported earlier by Allendorf and Spear [16]. In the first case, calculations for full equilibrium were performed (i.e., gas and liquid in equilibrium with crystalline silica). In the second case, the formation of stoichiometric crystalline phases (including all forms of SiO_2) was suppressed. This is the equivalent of placing an infinite kinetic barrier to the reaction of either the gas or the liquid with the silica grains. The Na_2O concentration was then determined at two fixed temperatures (1883 and 1765 K) corresponding to specific experimental data (see below) and over a range of input NaOH(g) activities (the activity is fixed so that the NaOH(g) concentration does not vary). The input composition for these calculations in all cases simulates an oxy-fuel combustion atmosphere (O_2/CH_4 mole ratio = 2.05, yielding an H_2O mole fraction ≈0.65).

The results in figure 5 show that for a gas/liquid partial equilibrium, the amount of Na_2O in the liquid is often much higher than that expected at full equilibrium. For example, at 1765 K, full equilibrium predicts that the liquid product will contain 5.5 % Na_2O, while gas/liquid partial equilibrium predicts values ranging from 5.6 % at 100 ppm NaOH(g) to 18.1 % at 200 ppm NaOH(g). Similarly, at

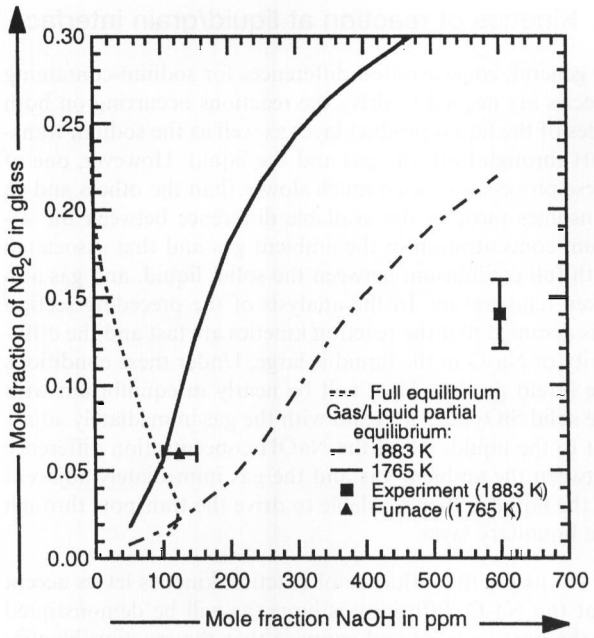

Figure 5. Comparison of measured and predicted concentrations of Na_2O in liquid corrosion product. Dashed line at left is a prediction based on complete equilibrium (gas + liquid corrosion product + silica). Solid and dash-dot lines sloping up to the right are predictions based on equilibrium between the liquid corrosion product and furnace gases only (i.e., no solid phases are allowed to form).

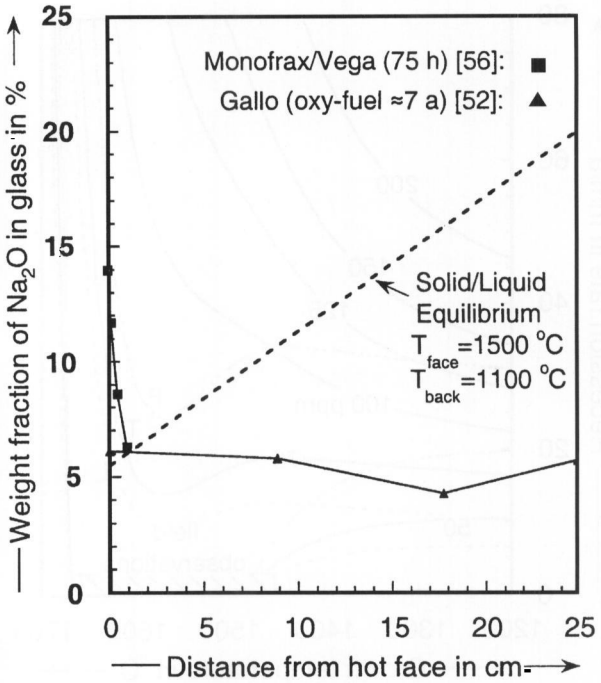

Figure 6. Na_2O content of glass corrosion product versus depth into worn silica bricks. Measured data (symbols) are from bricks extracted from a Gallo furnace (Moore, Neufeld and Wolfe [29]; Wolfe [56]) and from samples exposed in a Monofrax test furnace (Gupta [33]; Wolfe [52]). Na mole fraction in glass at Gallo brick surface is consistent with predictions (dashed line) based on equilibrium thermodynamics, but the data does not show the expected increase of Na content in the cooler brick interior. Na content at Monofrax brick surface exceeds prediction, perhaps because of relatively short duration of tests; interior Na content is consistent with Gallo data and with computed equilibrium.

1883 K, full equilibrium produces a liquid product with 2.1 % Na_2O, while gas/liquid partial equilibrium gives 1.6 % at 100 ppm NaOH(g) and 9.5 % at 200 ppm. Note that each point on the full equilibrium (dashed) curve in figure 5 corresponds to a particular temperature; this curve is equivalent to the oxy-fuel NaOH(g) versus temperature curve in figure 2, but rotated clockwise by ninety degrees. Note that this Na_2O mole fraction exceeds the full equilibrium value ($x(T, X_{NaOH(g)}) > x_{eq}(T)$) whenever the gas-phase NaOH(g) concentration exceeds its value at full equilibrium ($X > X_{eq}(T)$).

These predictions can be compared with measured Na_2O concentrations found in postmortem analyses of refractory samples recovered from glass-melting furnaces. We discuss one example in detail (shown in figures 5 and 6 by filled triangles), since we are fortunate to have fairly complete information concerning furnace conditions and the sample properties provided by Moore et al. [29]. Other data in the literature are in qualitative agreement, however (see below). The point shown in figure 5 represents the Na_2O concentration (obtained by energy dispersive spectroscopy (EDS)) of an amorphous phase that fills the pores of a brick[1)] salvaged from an oxy-fuel container-glass furnace producing soda-lime glass and operated for seven years (referred to below as the Moore et al. sample) [29]. The temperature of the brick, 1765 K (1492 °C), is assumed to be the same as that measured at a nearby breast-wall location using optical pyrometry [30]. As seen in figure 6, the measured Na_2O content of the glass within the brick pores is (5.5 ± 0.5) wt% through most of the 25-cm thickness of the remaining brick (the length of an unused brick was 38.1 cm). This measurement is in good agreement with the computed full equilibrium value (also 5.5 %) corresponding to a brick surface temperature of 1765 K, suggesting that the rate of reaction between Na_2O and the silica grains is not rate-limiting. In contrast, gas-liquid partial equilibrium yields a much higher Na_2O concentration. Assuming an NaOH(g) concentration of (125 ± 25) ppm based on the measurements of Walsh et al. [19], partial equilibrium predicts an Na_2O concentration in the liquid product of 9.0 mol%.

Since the Na_2O concentrations obtained from the postmortem analysis of the Gallo brick are fairly consistent with full equilibrium expectations, it appears that chemical-kinetic limitations are not limiting the long-term corrosion rates of silica bricks. An important qualification must be raised, however: the predicted equilibrium Na_2O concentration is rather sensitive to temperature, decreasing as temperature increases. For example, increasing the temperature by 50 K from 1765 to 1815 K decreases the predicted Na_2O concentration at full equilibrium from 5.5 to 3.9 mol%. This raises the possibility that the measured Na_2O concentration could exceed that at full equilibrium, suggesting that a moderate kinetic limitation could exist. Since the temperature used in

[1)] Gen-Sil (RHI Refractories). Analysis of unused brick (in wt%): 95.9 SiO_2, 2.8 CaO, 0.8 Fe_2O_3. Sample estimated to have come from approximately 5 m on centerline from the batch charger end wall of the furnace. For additional details on the furnace configuration, see reference 18 in [20]

the calculations actually corresponds to the breast wall of the furnace (albeit at the same distance down the furnace axis as the sample taken from the crown), an error of 50 K or even more does not seem unreasonable.

It is further seen in figure 6 that the measured Na_2O content in the cooler interior and back side of the Moore et al. sample (≈5.5 %) is well below the predicted equilibrium Na_2O content (dotted line, figure 6). The dotted line is based on an estimated back side temperature of around 1400 K, for which full equilibrium predicts 19 % Na_2O in the liquid product (see figure 2), in contrast with 5.5 % at the much hotter front surface. Since we believe that most of the glass is formed at the hot face and drawn into the brick pores (as explained later), it appears that a kinetic limitation may prevent the precipitation of silica from the liquid corrosion product so that its Na_2O concentration cannot increase to the equilibrium value corresponding to the cool interior. This is consistent with the fact that crystallization of silica from a melt is very difficult [31 and 32], particularly at the temperatures encountered here (< 1738 K) in which tridymite is the thermodynamically favored phase. There is no evidence to indicate, however, that this kinetic limitation, if it in fact exists, limits the rate of front-surface corrosion.

Data from Faber and Verheijen (FV) further supports the hypothesis that reaction kinetics do not limit long-term furnace corrosion rates. FV report measurements of Na_2O concentration in corroded silica samples [10], although the sample temperature during furnace operation is not given. Thus, we cannot perform equilibrium predictions corresponding to the operating conditions of the furnace. Nevertheless, the results are qualitatively consistent, showing a relatively constant Na_2O weight fraction throughout a 30-cm portion of the brick. If a porosity of 20 % (typical of porous silica refractories) is assumed, the FV weight fractions convert to mole fractions (2.5 to 4.4 mol%) that are comparable to those corresponding to the Moore et al. sample [29].

In contrast to the results of these long-term corrosion processes, laboratory measurements suggest that chemical-kinetic rate limitations may appear under experimental conditions in which the time scales are necessarily shorter than typical furnace campaigns. The square symbol in figure 6 represents an EDS measurement of Na_2O content in an amorphous phase similar to the Moore et al. sample, but found within the pores of a silica refractory sample exposed to a controlled atmosphere containing a gas mixture intended to simulate oxy-fuel conditions in a laboratory-scale furnace.[2)] The atmosphere contained (640 ± 65) ppm NaOH(g) and the test was conducted at 1883 K (1610 °C) for 75 h [33]. The measured Na_2O concentration of ≈14 % lies roughly midway between the values of 2.5 and 23 % that, respectively, apply for full equilibrium and gas/liquid partial equilibrium with 640 ppm NaOH(g). In this case, the liquid product is clearly not in equilibrium with crystalline SiO_2, since the Na_2O content is nearly six times greater than that predicted for full equilibrium. If such conditions persisted over extended periods of time in a full-scale furnace, the deviation from equilibrium would reduce the computed surface recession rate by a factor of about six, since the amount of NaOH(g) required to remove each mole of SiO_2 increases by that factor. However, it is seen in figure 6 that the glass samples from the interior of the ((25 x 25) mm^2 cross section) test samples have much lower Na_2O concentrations (≈6 %) more typical of the Gallo measurements and the equilibrium calculations.

In summary, the available measurements suggest that the liquid corrosion product produced at the surface of silica bricks under typical furnace operating conditions is reasonably consistent with predictions based on a full equilibrium between silica in the crown and the furnace gases immediately adjacent to it. However, interior Na_2O concentrations are considerably less than equilibrium values, suggesting a kinetic barrier to tridymite precipitation. A corollary to these conclusions is that laboratory experiments, even when they attempt to reproduce realistic furnace atmospheres, may not produce corrosion products whose composition mimics that found from post-mortem samples because the duration of such tests is typically much shorter than the lifetime of a refractory in a full-scale furnace.

5. Diffusion of Na_2O through the liquid product layer

Na_2O formed at the gas/liquid interface must be transported through the liquid product layer on the brick face to the liquid/solid contact by diffusion. Thus, in analogy with the previous analysis of gas-phase transport, the rate of recession is limited by the rate of diffusion through the liquid product layer.

$$\frac{dl}{dt} = \frac{\varrho_{liq}}{\varrho_{SiO_2}} \Delta x \frac{D_{Na_2O}}{\delta_l} \left(\frac{1 - x_r}{2 x_r} \right). \tag{16}$$

Here, Δx is the difference between the Na_2O concentrations in the liquid at the gas/liquid and liquid/solid interfaces.

$$\Delta x = x_{g,l} - x_{l,s} . \tag{17}$$

This difference is at its maximum when x_{gl} is in equilibrium with the furnace gas and $x_{l,s}$ is in equilibrium with the solid SiO_2. As noted earlier in figure 5, $x_{l,s}$ is a function of temperature alone whereas $x_{g,l}$ is a function of temperature and NaOH concentration. The mole fraction x_r in equation (16) is that of the melt being removed from the liquid layer. If the melt is dripping from the gas/liquid side of the layer, the melt being removed has a mole fraction of $x_r = x_{g,l}$ whereas the appropriate mole fraction is $x_r = x_{l,s}$ when the glass melt is being drawn into the pores of the brick. Note that in earlier discussion and in equations (1) and (4) we did not subscript the symbol x because it had been previously

[2)] Vega (RHI Refractories). Analysis of unused brick (in wt%): 96.4 SiO_2, 2.9 CaO, 0.5 Fe_2O_3. Tests performed in laboratory furnace at Monofrax Inc., Falconer, NY (USA). Combustion gases are simulated by burning a stoichiometric natural gas/oxygen mixture (4.25 standard liters per minute total flow rate) in a separate chamber. Hot combustion products from that chamber then flow into an insulated, isothermal chamber containing a bath of molten glass. In this case, soda-lime-silica cullet with the following composition (in wt%) typical of float glass was used: 72.7 SiO_2, 13.92 Na_2O, 0.5 K_2O, 8.6 CaO, 4.21 MgO. Refractory samples ((5 x 5 x 11) cm^3) were suspended above the glass bath on slabs of α,β-alumina. NaOH concentrations were determined using extractive sampling and off-line wet-chemical analysis. Corroded samples were analyzed offline using scanning electron microscopy/EDS to determine the atomic composition of the corrosion products.

assumed that the mole fraction was uniform across the liquid layer and so there was no need to distinguish the side of the layer from which the liquid was removed.

The maximum thickness of the liquid melt layer on the brick face can be estimated by application of the Rayleigh-Taylor criterion for stability of a thin film. Droplet formation is likely to occur when the thickness of the film exceeds a critical thickness defined by

$$\delta_{\text{crit}} = \left(B_{\text{n}} \frac{\sigma}{\Delta\varrho\, g} \right)^{1/2} \approx 2\ \text{mm} \tag{18}$$

where σ is the surface tension, $\Delta\varrho$ is the density difference between the liquid film and the adjacent gas, g is the gravitational constant, and $B_{\text{n}} \approx 0.687$ is a constant determined by stability analysis [34]. A maximum stable layer thickness of 2 mm corresponds to a surface tension of 300 mN/m, typical of SiO_2 at 1500 °C. This is only a few times greater than the surface tension of water at room temperature; for that case the stability limit is slightly less that 1 mm. This layer thickness is well below the cutoff wavelength of the Kelvin-Helmholtz instability [35] that is driven by shear forces imposed by the external gas velocity of ≈1 m/s, so Rayleigh-Taylor instability is the controlling consideration. The layer may, of course, be thinner than the critical thickness when most of the melt is being drawn into the brick face by capillarity or as a result of film flow down inclined portions of the crown. We will use the maximum thickness to show that diffusion through even the thickest possible layer cannot place a significant constraint on the rate of surface corrosion.

The maximum stable layer thickness is proportional to the square root of the surface tension which increases moderately with increasing temperature. For example, a temperature rise of 300 K increases the surface tension by only 10 % [36]. Increased water content in the layer reduces the surface tension, but again the changes appear moderate. An increase in water vapor mole fraction from 0 to 0.025 reduces the surface tension by only 10 % [36]. Moreover, an exponential extrapolation of this measured trend to a mole fraction of 0.5 (similar to oxygen/fuel fired conditions) provides less than a factor of two total reduction in surface tension. Although some studies show a weak variation of surface tension with Na_2O content, Kucuk et al. [37] find that these variations are not statistically significant. In addition, the stability limit does not depend on viscosity; this property only affects the growth rate of disturbances that lead to droplet formation. Thus, it appears likely that the stable layer thickness will be quite similar for air- and oxygen-fired conditions and independent of layer composition.

To our knowledge the diffusivity of Na_2O in silicate melts has not been directly measured at the temperatures of interest. Nor is there data concerning the dissociation of Na_2O and the diffusivity of all relevant ionic and molecular species. However, there is a great deal of information regarding the diffusivity of H_2O as well as Na, O, H, and OH ions. Much of this is found in the geophysical literature where there is considerable interest in silica-rich magmas, and these studies appear consistent with recent measurements by Mesko and Shelby [38] for commercial float glass and TV panel glass. In general, sodium ions are known to diffuse very readily, having a diffusivity approaching 10^{-4} cm^2/s at 1600 °C [39 and 40]. Oxygen species generally

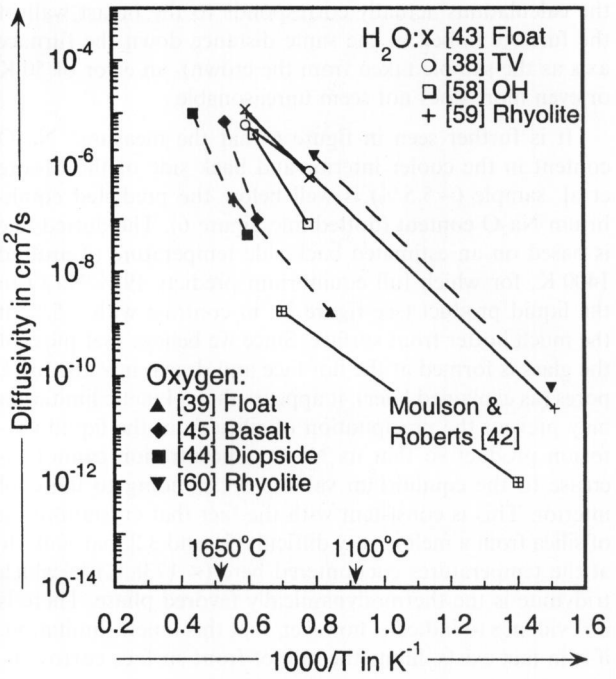

Figure 7. Measured diffusivities of oxygen species in silicate melts. Only the end points of the best fitting lines are shown. H_2O and O diffusivities are used to estimate the diffusivity of Na_2O through silicate melt layer on brick face. Recent data from Mesko and Shelby are most relevant to present study [38 and 43]. Other sources of data include Moulson and Roberts [42], McGinnis and Shelby [58], Zang and Behrens [59], Pfeiffer [39], Lesher et al. [45], Reid et al. [44] and Doremus [60].

diffuse much slower because they bond to silicon in the glass and must diffuse from one bond to another in the silicate network. Thus, the diffusion of Na_2O is likely to be limited by diffusion of oxygen species, suggesting that estimates can be made on the basis of previous studies addressing H_2O, O, and OH.

Figure 7 illustrates measured diffusivities of oxygen species in glass melts within the temperature range of interest. Perhaps the oldest and best known data set, that of Moulson and Roberts [41 and 42] lies far below the bulk of the data. The other measurements for oxygen and water are relatively consistent with one another, though order of magnitude variations are seen in both sets, perhaps for reasons that differentiate the particular experiments. The data most relevant to the present study is that of Mesko and Shelby for float glass [43]. At 1600 °C their H_2O diffusivity is around 10^{-5} cm^2/s, similar to that measured for oxygen by Reid [44] and by Lesher [45]. Ignoring Moulson and Roberts, the lowest estimate of diffusivity at 1600 °C is obtained by an extrapolation of Pfeiffer's data [39] to a value of about 10^{-6} cm^2/s, roughly tenfold less than Mesko and Shelby.

Computed recession rates limited only by diffusion of Na_2O through a 2-mm liquid film are shown in figure 8 for ambient NaOH concentrations of 80, 200, and 600 ppm. The upper and lower sets of calculations utilize the diffusivity estimates of Mesko and Shelby [43] and Pfeiffer [39] respectively. The upper set, thought to be the best estimate, is in reasonable agreement with recession rates observed by ORNL [46 and 47] and Corning [48] in crucible tests. Although the chemistry of these tests [49] differs from the

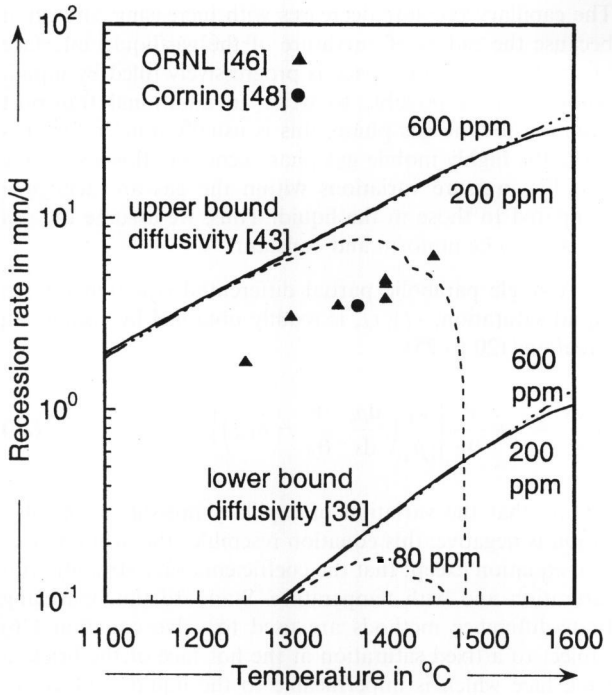

Figure 8. Computed recession rates limited only by Na_2O diffusion through a 2 mm silicate liquid layer on the brick face. Calculations (upper lines) based on diffusivity data of Mesko and Shelby [43] are similar to measured recession rates in crucible tests on standard silica bricks at Oak Ridge National Laboratories by Roberts and Pint [46] and at Corning by Brown et al. [48] Diffusion-limited recession rates greatly exceed those observed in field environment, even for lower bound estimates of diffusivity.

NaOH process that we are modeling, the gas in the crucible contains high concentrations of the reactant species and the corrosion rates are very large.

The most important conclusion to be drawn from figure 8 is that diffusion of Na_2O through the liquid product layer is not a controlling consideration in full-scale furnaces. First, the fact that crucible corrosion rates are as large as those observed by ORNL implies that the upper bound estimate of diffusivity, based on the Mesko and Shelby H_2O diffusion data [43], is substantially correct for diffusion of Na_2O in silicate melts. A smaller diffusivity could not support such high recession rates. Furthermore, based on the Mesko and Shelby diffusivity and an NaOH concentration of 100 to 200 ppm, maximum recession rates of 1 m/a would be attainable in the field. Since this greatly exceeds the earlier estimates based on gas phase transport, it follows that liquid phase diffusion is not the rate-controlling consideration in the corrosion process observed in the field.

The recession rates shown in figure 8 are computed from equations (16) and (17) using values of $x_{g,l}$ and $x_{l,s}$ shown in figure 5. In addition it is assumed that most of the liquid corrosion product drips from the liquid layer at high reaction rates and hence $x_r = x_{g,l}$. Liquid dripping from the hot side of the liquid layer has a high sodium content and so removes fewer moles of silica for each mole of Na, as compared with the lower sodium content of the silicate on the cooler side of the liquid layer, though these differences are only significant when there is a large variation of sodium content across the liquid layer. It is somewhat surprising to see that the computed recession rates are relatively insensitive to the amount of NaOH in the vapor phase. This is because the quantity, $f(X,T)$ below, that contains all of the thermodynamic information in equations (16) and (17), is relatively constant so long as the system is far from equilibrium.

$$f(X_{NaOH}, T) = (x_{g,l} - x_{l,s})\left(\frac{1 - x_r}{2x_r}\right)$$
$$\approx (x_{g,l} - x_{l,s})\left(\frac{1 - x_{g,l}}{2x_{g,l}}\right) \qquad (19)$$
$$\approx \left(\frac{1 - x_{g,l}}{2}\right) \approx \frac{1}{2}.$$

The second to the last of these approximations holds whenever the NaOH concentration is well above the equilibrium value and hence $x_{l,s} \ll x_{g,l}$. Further since $x_{g,l} < 0.3$ for the full range of conditions shown in figures 5 and 8, it follows that $f(X,T)$ never deviates substantially from 1/2, except in the immediate neighborhood of equilibrium. In this context, note that the predicted recession rate for 80 ppm dives abruptly to zero at a temperature of about 1480 °C where the gas approaches equilibrium with the solid.

The very comparable temperature dependence of the ORNL data [46 and 47] and the calculations in figure 8 suggest that liquid-phase diffusion is the controlling mechanism in their crucible tests. Further note that the slopes of most of the diffusivity data sets in figure 7 are comparable, suggesting similar activation energies that are all relatively consistent with the ORNL crucible data. Gas-phase transport of reactant species is apparently not an issue in the crucible tests, as compared with float-glass furnaces, because the crucible is nearly full of undiluted reactant gases that are continually replenished. In contrast, the NaOH gas concentration is orders of magnitude smaller in full-scale furnaces, and these gases must be transported from the glass surface to the crown, resulting in much more restrictive transport limitations on the corrosion rate.

6. Capillary suction of silicate melt into brick pores

The presence of silicate glass deep within porous bricks can be explained by two alternative mechanisms. The glass could be formed by chemical reaction of sodium with SiO_2 at the exposed brick face and the resulting liquid product subsequently drawn into the porous bricks, as we will argue here. Alternatively, sodium species could be transported to the brick interior where they react to form silicate glass. Some combination of these two mechanisms is also possible. However, it is unlikely that NaOH gas will have direct access to the interior of the brick since the surface pores are likely filled with silicate liquid and the brick surface is probably covered with a 1 to 2 mm liquid film for most of the life of the brick. NaOH can, of course, be dissolved in the liquid film to form Na_2O that is transported into the brick by liquid-phase diffusion. However since the equilibrium concentration of Na_2O in the melt increases with decreasing temperature, as apparent in figures 2 and 6, the equilibrium concentration gradient opposes the inward transport of

Na_2O. This objection could conceivably be overcome by departure from equilibrium, but this would imply very slow reaction kinetics and the available measurements of Na_2O concentrations suggest very flat concentration profiles on the interior. For these reasons we are inclined to believe that most of the silicate liquid is formed at the surface and drawn into the brick. In support of this hypothesis we now present calculations of liquid infiltration induced by capillary suction.

Two alternative models are used to compute the capillary suction of silicate liquid into a permeable brick. These may be viewed as bounding estimates as the first is based on a continuum description that emphasizes the role of the smaller pores while the second, a discrete capillary-bundle model, is dominated by the larger pores. In reality, the larger pores serve as conduits for transport of liquid that is drawn from these primary channels into surrounding pores of smaller size. So the expected behavior should lie within the bounds predicted by these two relatively simple models.

The continuum model outlined below is frequently applied to gas/liquid flows in oil fields and groundwater reservoirs [50]. Assuming for simplicity that no reactions occur on the brick interior, the mass of the liquid phase is conserved as it is transported inward, requiring that

$$\phi \varrho_l \frac{\partial s}{\partial t} = -\frac{\partial}{\partial y}(\varrho_l, u_l) . \tag{20}$$

Here, the liquid density, ϱ_l, and the brick porosity, ϕ, are taken as uniform and the saturation, s, represents the fraction or the local pore volume that is occupied by liquid. The remaining pore volume contains gas. The liquid velocity, u_l, may be written in the following Darcian form

$$u_l = -\kappa_l \frac{\kappa}{\mu}\left(\frac{\partial p_l}{\partial y} + \varrho_l g\right) \tag{21}$$

in which p_l is the liquid pressure, g is the gravitational constant, μ is the liquid viscosity, κ is the intrinsic permeability of the brick, and κ_l is the so-called relative permeability of the liquid. Lacking direct measurements of the intrinsic and relative permeabilities, we will utilize the commonly applied Karman-Cozney relationship and a relative permeability that increases as the square of the saturation (this latter variation is generally stronger than linear but weaker than cubic) [50 and 51].

$$\kappa = \frac{d_p^2}{180}\frac{\phi^3}{(1-\phi)^2} \tag{22}$$

$$\kappa_l = s^2 . \tag{23}$$

Here d_p is the mean pore diameter, taken as two microns based on the measured pores size distribution of a Gen-Sil brick [52]. The liquid and gas pressures differ by the capillary pressure, p_c, which is related to the surface tension, σ, and the radius of curvature, r, of the gas liquid interface.

$$p_c = p_g - p_l \tag{24}$$

$$p_c(s) = \frac{\sigma}{r(s)} . \tag{25}$$

The capillary pressure decreases with increasing saturation because the radius of curvature of the gas/liquid interface increases as the pore space is progressively filled by liquid. Although it is possible to write an additional transport equation for the gas phase, this is usually unnecessary because the highly mobile gas phase generally flows so freely that the pressure variations within the gas are negligible compared to those in the liquid. Thus, we assume the gas pressure to be uniform and constant.

A single parabolic partial differential equation for the liquid saturation, $s(y, t)$, is readily obtained by combining equations (20 to 25).

$$\phi \frac{\partial s}{\partial t} = -\kappa \frac{\partial}{\partial y}\left[\frac{\kappa_l}{\mu}\left(\frac{dp_c}{ds}\frac{\partial s}{\partial y} - \varrho_l g\right)\right] . \tag{26}$$

Noting that the variation of capillary pressure with saturation is negative, this equation resembles the heat conduction equation except that the coefficients vary strongly with saturation and with temperature. Standard time-marching finite-difference methods are used to solve equation (26) subject to a fixed saturation at the hot face of the brick, a back face which is impermeable to the liquid, and an initially dry pore space.

An alternative discrete-capillary model of liquid intrusion treats the pore space of the brick as a collection of independent capillary tubes [50 and 51]. For each pore size, the instantaneous rate of intrusion, dl_{liq}/dt, is equal to the liquid speed, u_l, given by the well-known Poiseulle relationship for flow in a circular channel [53] of diameter d_p driven both by gravity and by the pressure gradient induced by capillary suction.

$$u_l = \frac{dl_{liq}}{dt} = -\frac{d_p^2}{36}\frac{1}{\mu}\left(\frac{\partial p_l}{\partial y} + \varrho_l g\right) = \frac{d_p^2}{36}\frac{1}{\bar{\mu}}\left(\frac{p_c}{l_{liq}} - \varrho_l g\right) \tag{27}$$

Since the liquid speed along each capillary must be independent of axial position, the differential form of equation (26) can be readily integrated to obtain the final algebraic form containing the mean viscosity, $\bar{\mu}$, and the overall difference in liquid pressure along the capillary, p_c. At each time step of a simulation, velocities are computed for all pore sizes in the selected pore size distribution and these are used to compute the new penetration depth for each pore. As the infiltration speed depends on the mean viscosity, $\bar{\mu}$, along the entire wetted length of a given capillary, the corresponding fluid speed is greatly reduced as the fluid advances into cooler regions of the brick. The fluid saturation at any given depth into the brick is obtained by summing the pore volumes of all of the pores that are full to that depth. A key input to this analysis is the pore size distribution indicating the fraction of the total porosity associated with each pore size.

A typical capillary pressure curve and the corresponding pore size distribution are shown in figure 9. The capillary pressure variation [52] for mercury injection measurements was adjusted to account for the difference in surface tension between mercury and silicate liquids. The sample was taken from the back part of a brick that had been exposed for seven years in a Gallo oxygen/air furnace. Thus, the alterations of the pore structure are less than in other samples

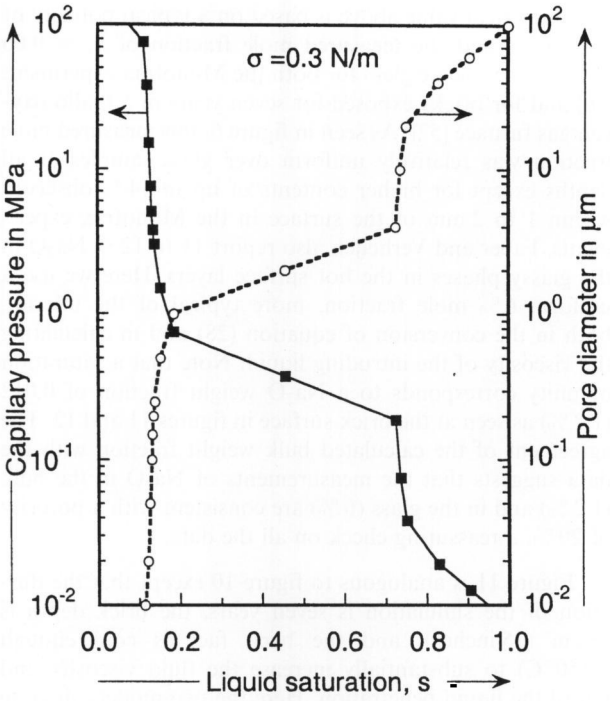

Figure 9. Variation of capillary pressure with liquid saturation derived from mercury injection measurements reported by Wolfe [56]. Values of the capillary pressure were measured as a function of incremental injection volume (equivalent to changes in saturation); corresponding values of pore sizes are computed. About 50 % of the pore volume resides in pores having diameters of 1 to 4 μm; mean pore diameter is around 2 μm.

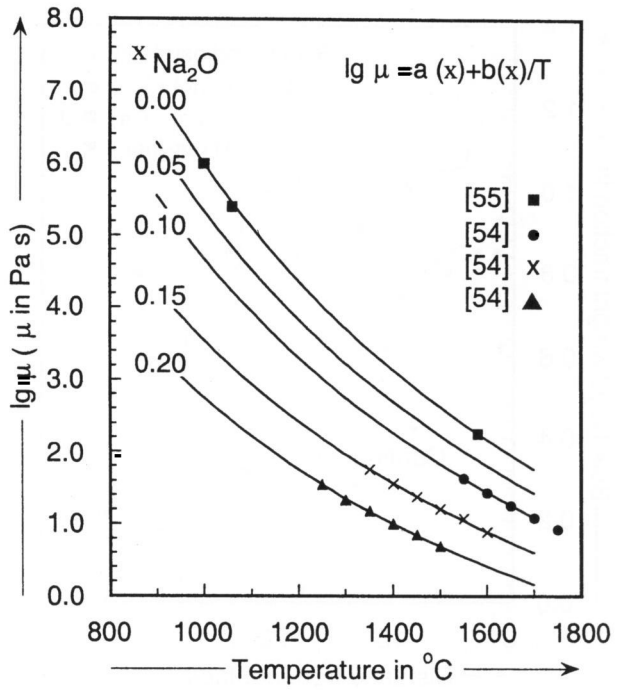

Figure 10. Variation of silicate liquid viscosity with temperature for Na_2O mole fractions ranging from 0.0 to 0.20. Experimental data of Heatherington and Jack [55] and Bockris et. al [54] are well approximated by fitting functions that vary exponentially with absolute temperature.

that were closer to the hot face. Although it is not clear how typical this brick might be, it should be useful as a guideline in demonstrating the probable liquid intrusion distance under typical operating conditions.

The fluid viscosity is another key input to both the transport models, continuum and discrete. The measured variation of viscosity with temperature and Na_2O mole fraction [54 and 55] is well approximated by the analytical approximations (solid lines) shown in figure 10. Two-parameter exponential fitting functions were developed for each of the five mole fractions displayed in the plot. Viscosities corresponding to mole fractions intermediate between these five curves are estimated by linear interpolation. Note that the viscosity increases by about four orders of magnitude as the temperature falls from the hot face (≈1600 °C) to the cold face (≈1100 °C) greatly reducing the intrusion speed of the glass melt as it approaches the back face.

Figure 11 compares the results of a typical liquid intrusion simulation with the measured intrusion in laboratory experiments by Gupta [33] and by Faber and Beerkens (FB98) [17]. In both experiments the temperature and NaOH vapor concentration were around 1600 °C and 600 ppm. The samples used by Gupta were rectangular bars having a (50 x 50) mm^2 cross section, while the simplified one-dimensional models assumes symmetry about a midplane 25 mm from the exposed face. The FB98 samples were deeper but the infiltration depth observed after 20 h was small enough to admit the same simplified model. Since Gupta's samples were essentially isothermal and the measured intrusion was small in the FB98 experiments, the calculation assumes a uniform brick temperature of 1600 °C.

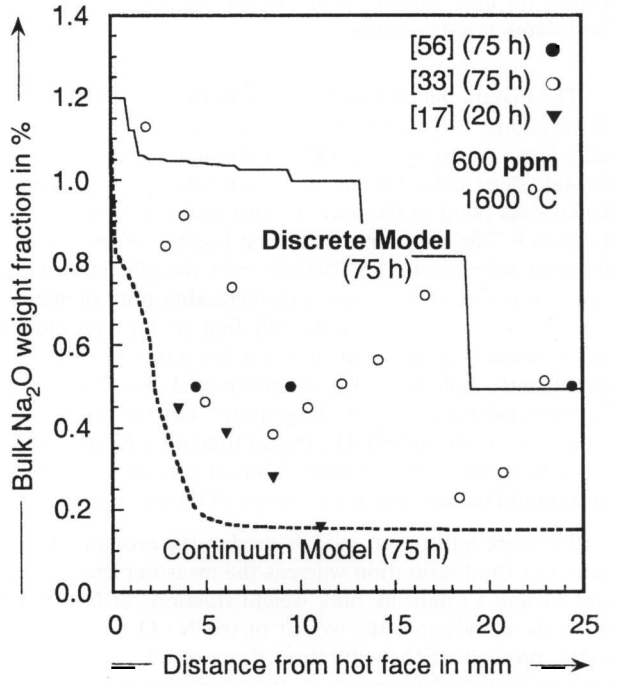

Figure 11. Comparison of measured (symbols) and computed liquid intrusion in a silica brick at a uniform temperature of 1600 °C. Corresponding experimental data are from a 20 h test by Faber and Beerkens [17] and a 75 h test reported by Gupta [33] and Wolfe [56]. Discrete and continuum model predictions are for 75 h. Measurements are bounded by results of discrete capillary-bundle model and continuum model, suggesting that liquid can be drawn into observed depths by capillary suction.

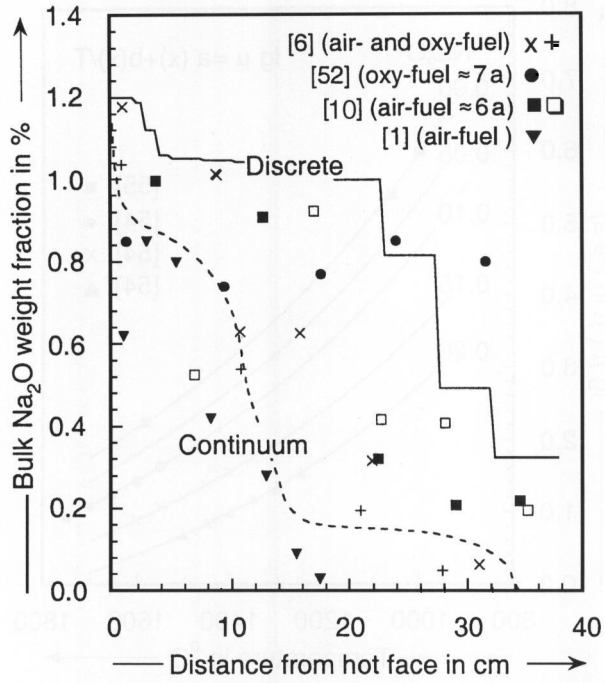

Figure 12. Comparison of measured (symbols) and computed Na_2O profiles in a silica brick having front and back face temperatures of 1600 and 1050 °C. Corresponding experimental data are from worn bricks from long campaigns examined by Reich [1], Wolfe (Gallo furnace) [52], Faber and Verheijen [10] (open symbols 1580 °C, filled symbols 1530 °C) and Paskocimas et al. [6] (+ sidewall, x crown). Pore size distribution and viscosity used in calculation are the same as in figures 9 and 10. Continuum (dashed line) and discrete (solid) models provide bounds on data similar to those observed for smaller-scale short-duration experiments.

The two modeling results shown in figure 11 bound the observations. The discrete capillary model predicts substantially greater intrusion than the continuum model. Each of the stair-steps in the discrete prediction corresponds to a particular data point in the pore size distribution shown earlier in figure 9. The largest pores fill first because of their larger diameter reduces viscous friction, even though the driving capillary pressure decreases with increasing pore diameter. Conversely, the smallest pores fill first in the continuum model because dp_c/ds is greatest for low saturations corresponding to small pores. The discrete model is correct in predicting rapid intrusion into large pores, but the rate of advance is in reality curtailed by loss of fluid into the surrounding material with smaller pores. Thus, it is expected that the data should fall between the extremes of the two models.

The pore infiltration models predict the evolving distribution of fluid saturation whereas the measurements in figures 11 and 12 indicate bulk weight fractions of Na_2O. To make the conversion, the weight of the Na_2O is computed as the product of the saturation (fraction of pore volume filled by liquid), the porosity, ϕ, the weight fraction of Na_2O in the liquid, x_r, (same as the mole fraction since molecular weights of Na_2O and SiO_2 are essentially the same), and the liquid density. The total weight includes the liquid and the SiO_2.

$$\frac{W_{Na_2O}}{W_{total}} = \frac{s\,\phi\,x_r\,\varrho_{liq}}{s\,\phi\,\varrho_{liq} + (1-\phi)\varrho_{SiO_2}} \approx s\,\phi\,x_r \approx 0.012\,s\,. \quad (28)$$

The numerical value above is based on a typical porosity of 0.2 (20 %) and the measured mole fraction of $x_r = 0.06$ (6 %) in the silicate glass for both the Monofrax experiment [56] and for bricks exposed for seven years in a Gallo oxygen/gas furnace [52]. As seen in figure 6, this measured mole fraction was relatively uniform over glass samples at all depths except for higher contents of up to 14 % observed within 1 to 2 mm of the surface in the Monofrax experiments. Faber and Verheijen also report 11 to 12 % Na_2O in the glassy phases in the hot surface layers. Here we use a uniform 6 % mole fraction, more typical of the interior, both in the conversion of equation (28) and in calculating the viscosity of the intruding liquid. Note that a saturation of unity corresponds to a Na_2O weight fraction of 0.012 (1.2 %) as seen at the brick surface in figures 11 and 12. The agreement of the calculated bulk weight fraction with the data suggests that the measurements of Na_2O in the bulk (1.2 %) and in the glass (6 %) are consistent with a porosity of 20 %, a reassuring check on all the data.

Figure 11 is analogous to figure 10 except that the duration of the simulation is seven years, the brick depth is 38 cm (15 inches), and the back face is cool enough (1150 °C) to substantially increase the fluid viscosity and retard the liquid penetration. Here the two models, discrete and continuum, are in somewhat better agreement with one another and with the measured data from a number of diverse sources. It is interesting to note in figure 12 that the bricks exposed to air/fuel combustion appear to have about 20 to 50 % of their total porosity filled with liquid corrosion products. For a 38 cm brick with 15 % to 20 % porosity, this volume of liquid corresponds to a front face recession ranging from about 1 to 4 cm (3 to 12 % of the length), roughly consistent with field observations. The pore volume of the Gallo brick [27] appears to be about 70 % full, corresponding to a recession of about 5 cm. The observed recession was greater than this, suggesting that most of the corroded material dripped from the brick in late stages of the process.

The primary conclusion to be drawn from these comparisons of calculations with data is that capillary infiltration is the probable explanation for observed levels of Na_2O deep within worn bricks. Precise comparisons are not to be expected since the intrusion depends on the liquid and solid composition, chemical interactions, pore size distribution, capillary pressure, pore connectivity, and micro structural details that are difficult to measure and even more difficult to incorporate into brick-scale calculations that span years of operation. Fortunately, there is generally little need for such knowledge. The only observable or detrimental influence of liquid intrusion is that dripping will occur when the rate of intrusion is slower than the rate of liquid production at the surface. The onset of dripping and the drip rate could be estimated by application of the preceding models of surface recession and liquid intrusion.

7. Summary and conclusions

This paper presents the first comprehensive analysis of the transport and chemical mechanisms that are potentially active in the corrosion of porous refractories used to line the crowns of glass melting furnaces. The work focuses on low-density silica refractory because of its extensive use through-

out the glass industry and because of the serious corrosion problems that are observed for this material under some conditions. However, the nature of the analysis is such that these results can be extended to any refractory, assuming that a thermodynamic model is available to describe the chemical reaction between a gas-phase reactant, such as NaOH or KOH, and the refractory surface.

The results can be summarized briefly as follows: of the four mechanisms examined, only gas-phase transport of reacting species (in this case, NaOH) through a concentration boundary layer adjacent to the refractory hot face and a chemical-kinetic limitation at the surface of a silica particle appear to be realistic rate-limiting steps. Diffusion of reactant sodium, presumably as Na_2O, through a liquid product layer is far too fast to be rate-limiting under furnace conditions. Similarly, the analysis of capillary suction indicates that liquid sodium silicates will rapidly fill the small pores deep within a porous silica brick and thus block the intrusion of gas-phase species from entering and reacting.

Although computed corrosion rates based on mass transport through a gas boundary layer are somewhat greater than those observed, the results are very sensitive to the gas-phase concentration of NaOH and to the refractory temperature, both of which contain significant uncertainties. Similarly, lack of precise knowledge concerning the refractory temperature, which is almost certainly somewhat cooler than the combustion gases near it, affects the accuracy of thermodynamic calculations used to predict the sodium content of the corrosion product, which again affects the predicted corrosion rate. Clearly, these results point to the need for improved measurements of both temperature and NaOH concentration in full-scale furnaces. Based on the (admittedly limited) laboratory data presented here, it appears that extrapolation of short-duration experiments to the determination of long-term corrosion rates is problematic. Time-dependent effects, possibly the result of finite-rate chemical kinetics, may alter the composition of observed corrosion products, yielding results that differ from equilibrium predictions that seem to be valid at the very long lifetimes experienced by refractory bricks in full-scale furnaces.

Despite these uncertainties, the foregoing analysis provides considerable insight into the corrosion process and should be helpful in furnace design and optimization. In particular, the analytical models developed here can be incorporated as submodels within full-scale furnace CFD codes; an effort to do this is underway. Furthermore, since corrosion appears to occur mainly at the crown hot face, the presence of pores in the refractory should have relatively little effect on the corrosion rate while at the same time providing suction of corrosion products into the bricks, substantially reducing dripping into the glass melt. Hence, the desirable features of low-density refractory, in particular its low thermal conductivity and weight, could be retained in an improved brick whose chemical reactivity toward gas-phase alkali is lower than that of silica.

*

The authors wish to acknowledge the following individuals for their very generous support of this project: Amul Gupta (Monofrax Inc., Falconer, NY) for conducting laboratory corrosion tests and analysis; RHI Refractories, in particular H. E. Wolfe, for providing extensive analysis of corroded refractory samples; and R. D. Moore and J. Neufeld (Gallo Glass Co., Modesto, CA) for providing detailed information concerning operating conditions and the design of the Tank 1 oxy-fuel furnace. This work was supported by the U.S. Dept. of Energy (DOE) Office of Industrial Technologies Glass Industry of the Future Team, American Air Liquide, BOC Gases, PPG Industries Inc., Praxair Inc., Techneglas, and Visteon Automotive Systems.

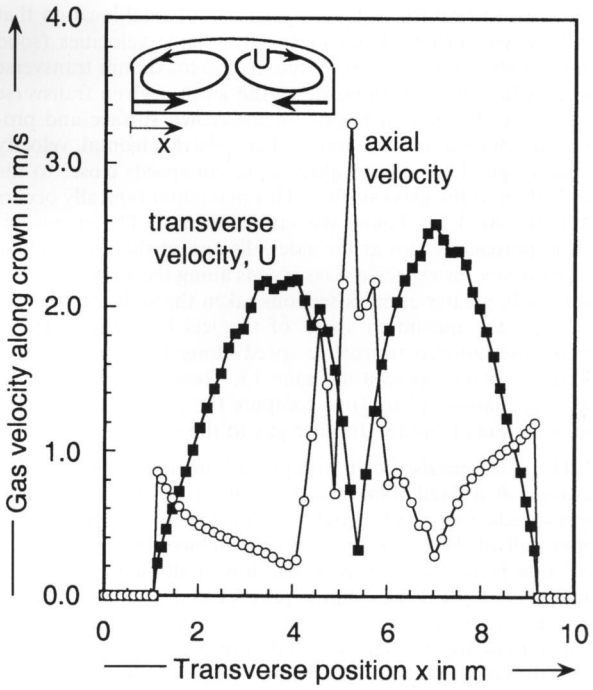

Figure 13. Computed transverse and axial speeds near the crown of a Gallo oxy/fuel furnace. Convective roll cells are driven by opposing combustion jets. Maximum tangential speeds typically occur about 0.2 to 0.3 m below the crown surface and are on the order of 1.5 m/s. Numerical values shown are obtained by post-processing of numerical simulations performed by Air Liquide.

8. Appendix: CFD calculations of furnace-scale transport

Gas velocities, temperature, and NaOH concentrations within furnaces are important input to the analytical models described in this paper. Since these data are often not available, it was necessary to compute them using a numerical furnace model developed by Air Liquide [57]. This model solves the governing Navier-Stokes, species transport, and energy-transport equations, yielding detailed three-dimensional distributions of gas velocity, temperature, and chemical composition. Calculations were first performed to provide contour plots of gas velocity and shear stress adjacent to the crown for typical cases of high-momentum and low-momentum burners [57]. A second set of calculations addresses a particularly well-documented furnace configuration, Gallo Glass Co. Tank 1 furnace, which uses oxygen to support combustion; this furnace is the source of the Moore et al. post-mortem samples discussed above [29]. It is heated by four pairs of burners that direct combustion gases from opposite sidewalls toward the furnace center.

As indicated schematically in the inset of figure 13, the opposing burner jets produce a pair of counter-rotating convective rolls having inward velocities along the glass surface and outward velocities along the crown. Figure 13 also shows the maximum transverse or tangential velocity near the crown surface

for a cross section through the furnace at an axial location that lies between burners. Each of the transverse velocities (solid symbols) shown in the plot represents the maximum transverse speed in the direction opposite to the jet at a given transverse position, x. The search begins on the crown surface and proceeds downward to the point where the horizontal velocity changes sign. Thus, these values represent speeds closer to the crown than to the glass surface. This maximum typically occurs about 0.2 to 0.3 m below the crown surface. The transverse speed approaches zero at the sidewalls and at the center plane of the furnace, as expected. Gas speeds along the crown are only moderately greater at cross sections taken through the burners. Although the maximum speed of the jets is in the order of 30 m/s, the induced transverse speed along the crown is only about 1 to 2 m/s, as seen in figure 13. These gas velocities are used in equations (2 to 7) to compute the rate of transport of sodium vapors from the furnace gas to the crown surface.

The axial speeds shown in figure 13 are again maxima over elevation at a fixed transverse location, x. As with the transverse speeds, the search is only extended over elevations in the upper half of the convective roll cells induced by the jets. The axial flow is induced mainly by the flow of all the injected combustion gas toward the exhaust port located at one end of the furnace. For the most part, axial flow speeds are considerably smaller than the transverse speeds driven by the burner jets. Thus, the convective roll cells and associated transverse or tangential gas velocities are of principal importance in the furnace-scale transport of NaOH gas from the glass surface to the crown.

9. References

[1] Reich, H. F.: Über einige Untersuchungen an Silika-Gewölbesteinen aus Glaswannen mit unterschiedlichen Arbeitstemperaturen. Glastechn. Ber. **34** (1961), pp. 15–27.

[2] Morsanyi, A. V.: Silica brick in the superstructure of glass-melting furnaces. Pt 2. Corrosion of silica brick in the superstructure and crowns of glass-melting furnaces. Glass Technol. **7** (1966) pp. 196–202.

[3] Morsanyi, A. V.: Silica brick in the superstructure of glass-melting furnaces. Pt 1. Corrosion of silica brick by the vapour of sodium salts. Glass Technol. **7** (1966) pp. 193–196.

[4] LeBlanc, J.: Controlling silica attack on soda lime oxy-fuel furnaces. Ceram. Ind. (1996) pp. 27–29.

[5] Gridley, M.: Philosophy, design, and performance of oxy-fuel furnaces. Ceram. Eng. Sci. Proc. **18** (1997) pp. 1–14.

[6] Paskocimas, C. A.; Leite, E. R.; Longo, E. et al.: Determination of corrosion factors in glass furnaces. Ceram. Eng. Sci. Proc. **19** (1998) pp. 75–88.

[7] Kotacska, L. H.; Cooper, T. J.: Testing of superstructure refractories in a gas-oxy atmosphere against high-alkali glasses. Ceram. Eng. Sci. Proc. **18** (1997) pp. 136–145.

[8] Boillet, J.; Kobayashi, W.; Snyder, W. J. et al.: Corrosion of silica and mullite refractories use in glass furnaces under 100 % oxy-firing process. Ceram. Eng. Sci. Proc. **17** (1996) pp. 180–190.

[9] Boillet, J.; Paskocimas, C. A.; Leite, E. R. et al.: The influence of oxy-fuel combustion atmosphere in glass furnaces on refractory corrosion. In: Pecoraro, G. A. et al. (eds.): Corrosion of materials by molten glass. Vol.78. Westerville, OH: American Ceramic Society, 1996. Pp. 217–237.

[10] Faber, A. J.; Verheijen, O. S.: Refractory corrosion under oxy-fuel firing conditions. Ceram. Eng. Sci. Proc. **18** (1997) pp. 109–119.

[11] Godard, H. T.; Kotacska, L. H.; Wosinski, J. F. et al.: Refractory corrosion behavior under air-fuel and oxy-fuel environments. Ceram. Eng. Sci. Proc. **18** (1997) p. 180.

[12] Duvierre, G.; Zanoli, A.; Boussant-Roux, Y. et al.: Selection of optimum refractories for the superstructure of oxy-fuel glass melting furnaces. Ceram. Eng. Sci. Proc. **18** (1997) pp. 146–163.

[13] Tong, S. S. C.; Brown, J. T.; Kotacska, L. H.: Determination of trace impurities in a furnace atmosphere at operating temperature. Ceram. Eng. Sci. Proc. **18** (1997) pp. 208–215.

[14] Wu, K. T.; Kobayashi, H.: Three dimensional modeling of alkali volatization/crown corrosion in oxy-fired glass furnaces. In: Pecoraro, G. A. et al. (eds.): Corrosion of materials by molten glass. Vol.78. Westerville OH: American Ceramic Society, 1996. Pp. 205–216.

[15] Misra, M. K.; Tong, S. S. C.; Brown, J. T.: Superstructure corrosion in glass tanks: comparison of mathematical model with field measurements. Ceram. Eng. Sci. Proc. **19** (1998) pp. 137–143.

[16] Allendorf, M. D.; Spear, K. E.: Thermodynamic analysis of silica refractory corrosion in glass-melting furnaces. J. Electrochem. Soc. **148** (2001) pp. B59–B67.

[17] Faber, A. J.; Beerkens, R. G. C.: Reduction of refractory corrosion in oxy-fuel glass furnaces. In: Proc. XVIII International Congress on Glass, San Francisco, CA 1998. Westerville, OH: American Ceramic Society, 1998. (Publ. on CD-ROM.)

[18] Walsh, P. M.; Moore, R. D.; Neufeld, J. et al.: Sodium volatilization and silica refractory corrosion in an oxygen/natural-gaso-fired soda-lime-silica glass melting furnace. In: Ext. Abstracts: XIX International Congress on Glass, Edinburgh, Scotland 2001. Sheffield: Society of Glass Technology, 2001. Pp. 134–135.

[19] Walsh, P. M.; Moore, R. D.: Na vapor and gas temperature measured in glass container furnaces. The Glass Researcher **10** (2000) pp. 3–4.

[20] Buckley, S. G.; Walsh, P. M.; Hahn, D. W. et al: Measurements of sodium in an oxygen-natural gas-fired soda-lime glass melting furnace. Ceram. Eng. Sci. Proc. **2** (2000) pp. 183–205.

[21] Rohsenow, W. M.; Choi, H. Y.: Mass and momentum transfer: Englewood, NJ: Prentice-Hall, 1961.

[22] Bird, R. B.; Stewart, W. E.; Lightfoot, E. N.: Transport phenomena. New York. Wiley, 1960.

[23] Hirschfelder, J. O.; Curtiss, C. F.; Bird, R. B.: Molecular theory of gases and liquids. New York: Wiley, 1954.

[24] van Limpt, J. A. C.: Volatilisation in glass furnaces. An experimental tool to predict emissions of volatile species in industrial glass furnaces. In: Proc. International Commission on Glass – Annual Meeting, Amsterdam 2000.

[25] Wereszczak, A.; Wang, H.; Karakus, M. et al.: Postmortem analysis of salvaged conventional silica bricks from glass production furnaces. Glastech. Ber. Glass Sci. Technol. **73** (2000) pp. 165–174.

[26] Webb, B. W.: Measuring and modeling combustion in glass melting furnaces. Glass Researcher **6** (1997) pp. 16–18.

[27] ChemSage™ 4.1. GTT Technologies, Herzogenrath, Germany: 1998.

[28] Eriksson, G.; Hack, K.; SGTE Pure Substance Database, 1996 Version. Produced by the Scientific Group Thermodata Europe and obtained through GTT Technologies, Herzogenrath, (Germany).

[29] Moore, R. D.; Neufeld, J.; Wolfe, H. E., pers. comm., 2000.

[30] Wu, K. T., Praxair Inc., pers. comm., 2001.

[31] Hummel, F. A.: Introduction to phase equilibria in ceramic systems. New York: Dekker, 1984.

[32] Sosman, R. B.: The Phases of silica. New Brunswick, NJ: Rutgers University Press, 1965.

[33] Gupta, A., Monofrax Inc., pers. comm., 2000.

[34] Yiantsios, S. G.; Higgins, B. G.: Rayleigh-Taylor instability in thin viscous films. Phys. Fluids **A1** (1989) pp. 1484–1501.

[35] Chandrasekhar, S.: Hydrodynamic and hydromagnetic stability. Oxford: Clarendon Press, 1961.

[36] Kucuk, A.; Clare, A. G.; Jones, L. E.: Influence of various atmospheres on the surface properties of silicate melts. Glastech. Ber. Glass Sci. Technol. **73** (2000) pp. 123–129.

[37] Kucuk, A.; Clare, A. G.; Jones, L. E.: An estimation of the surface tension for silicate melts at 1400 °C using statistical analysis. Glass Technol. **40** (1999) pp. 149–153.
[38] Mesko, M. G.; Shelby, J. E.: Solubility and diffusion of water in melts of a TV panel glass. Phys. Chem. Glasses **42** (2001) pp. 17–22.
[39] Pfeiffer, T.: Viscosities and electrical conductivities of oxidic glass-forming melts. Sol. State Ionics **105** (1998) pp. 277–298.
[40] Schaeffer, H. A.: Diffusion controlled processes in glass forming melts. J. Non-Cryst. Sol. **67** (1984) pp. 19–33.
[41] Moulson, A. J.; Roberts, J. P.: Water in silica glass. Trans. Br. Ceram. Soc. **59** (1960) pp. 388–399.
[42] Moulson, A. J.; Roberts, J. P.: Water in silica glass. Trans. Faraday Soc. **57** (1961) pp. 1208–1216.
[43] Mesko, M. G.; Shelby, J. E.: Water solubility and diffusion in melts of commercial silicate glasses. Glastech. Ber. Glass Sci. Technol. **73 C2** (2000) pp. 13–22.
[44] Reid, J. E.; Poe, P. T.; Rubie, D. C. et al.: The self-diffusion of silicon and oxygen in diopside liquid up to 15 GPa. Geochim. Cosmochim. Acta **174** (2001) pp. 77–86.
[45] Lesher, B. E.; Hervig, R. L.; Tinker, D.: Self diffusion of network former (silicon and oxygen) in naturally occurring basaltic liquids. Geochim. Cosmochim. Acta **60** (1996) pp. 405–413.
[46] Roberts, C. D.; Pint, B. A., pers. comm., 1998.
[47] Wereszczak, A. A.; Karakus, M.; Liu, K. C. et al.: Compressive creep performance and high temperature dimensional stability of conventional silica refractories. Oak Ridge National Laboratories report ORNL/TM-13757, 1999.
[48] Brown, J. T.; Spaulding, R. F.; Whittemore, D. S. et al.: New silica refractory of oxy/fuel glass melting. In: Proc. XV Conference of Italian Association of Glass Technologists, Parma 1999. Int. J. Glass. Pp. 120–128.
[49] Prior, H. D.; McIntyer, D. A.; Bonsall, S. B.: A test procedure to characterize refractories for oxy-fuel fired glass furnace crown applications. In: Proc. 6th Unified International Technical Conference on Refractories, Berlin 1999. Pp. 230–233.
[50] Scheidegger, A. E.: The physics of flow through porous media. Toronto: University of Toronto Press, 1974.
[51] Dullien, F. A. L.: Porous media: fluid transport and pore structure. New York: Academic Press, 1979.
[52] Wolfe, H. E.: Laboratory Report #PD-0398 on Gen-Sil Silica Brick (from Gallo 7-year oxygen/fuel campaign). Harbison Walker Refractories Co., Garber Research Center report PD-0398, 2000.
[53] Schlichting, H.: Boundary layer theory. New York: McGraw Hill, 1968.
[54] Bockris, J. O. M.; Mackenzie, J. D.; Kitchener, J. A.: viscous flow of silica and binary liquid silicates. Faraday Soc., London Trans. **51** (1955) pp. 1734–1748.
[55] Hetherington, G.; Jack, K. H.: Water in vitreous silica. I. Influence of water content on the properties of vitreous silica. Phys. Chem. Glasses **3** (1962) pp. 129–133.
[56] Wolfe, H. E.: Laboratory Report PD-0396 on Silica Brick and Castables: Vega, VegaO2, Visil, and H-W Crownseal I. Harbison Walker Refractories Co., Garber Research Center report PD-0396, 1999.
[57] Ammouri, F.; Champinot, C.; Béchara, W. et al.: Influence of oxy-firing on radiation transfer to the glass melt in an industrial furnace: imporance of spectral radiation model, Glastech. Ber. Glass Sci. Technol. **70** (1997) pp. 201–206.
[58] McGinnis, P. B.; Shelby, J. E.: Diffusion of water in float glass melts. J. Non-Cryst. Solids **177** (1994) pp. 381–388.
[59] Zhang, Y.; Behrens, H.: H_2O diffusion in rhyolitic melts and glasses. Chemical Geology **169** (2000), p. 243–262.
[60] Doremus, R. H.: Diffusion of water in thyolite glass: diffusion-reaction model. J. Non-Cryst. Solids **261** (2000) pp. 101–107.

E303P006

Contact:

Dr. Mark Allendorf
Sandia National Laboratories
PO Box 969, MS 9052
Livermore, CA 94551-0969
USA

E-mail: mdallen@sandia.gov